Deriving ice thickness, glacier volume and bedrock morphology of the Austre Lovénbreen (Svalbard) using Ground-penetrating Radar

A. Saintenoy*, J.-M. Friedt†, A. D. Booth‡‖, F. Tolle§, É. Bernard§,
D. Laffly¶, C. Marlin* and M. Griselin§

*IDES, UMR 8148 CNRS, Université Paris Sud, Orsay, France
Email: albane.saintenoy@u-psud.fr

†FEMTO-ST, UMR 6174 CNRS, Université de Franche-Comté, Besançon, France

‡Glaciology Group, Department of Geography, Swansea University, Swansea, Wales, UK

§THÉMA, UMR 6049 CNRS, Université de Franche-Comté, Besançon, France

¶GEODE, UMR 5602 CNRS, Université de Toulouse, Toulouse, France

‖Now at: Department of Earth Science and Engineering, Imperial College London, South Kensington Campus, London, SW7 2AZ, UK

Abstract

The Austre Lovénbreen is a 4.6 km^2 glacier on the Archipelago of Svalbard (79^{o}N) that has been surveyed over the last 47 years in order of monitoring in particular the glacier evolution and associated hydrological phenomena in the context of nowadays global warming. A three-week field survey over April 2010 allowed for the acquisition of a dense mesh of Ground-penetrating Radar (GPR) data with an average of 14683 points per km^2 (67542 points total) on the glacier surface. The profiles were acquired using a Malå equipment with 100 MHz antennas, towed slowly enough to record on average every 0.3 m, a trace long enough to sound down to 189 m of ice. One profile was repeated with 50 MHz antenna to improve electromagnetic wave propagation depth in scattering media observed in the cirques closest to the slopes. The GPR was coupled to a GPS system to position traces. Each profile has been manually edited using standard GPR data processing including migration, to pick the reflection arrival time from the ice–bedrock interface. Snow cover was evaluated through 42 snow drilling measurements regularly spaced to cover all the glacier. These data were acquired at the time of the GPR survey and subsequently spatially interpolated using ordinary kriging. Using a snow velocity of 0.22 m/ns, the snow thickness was converted to electromagnetic wave travel-times and subtracted from the picked travel-times to the ice–bedrock interface. The resulting travel-times were converted to ice thickness using a velocity of 0.17 m/ns. The velocity uncertainty is discussed from a common mid-point profile analysis. A total of 67542 georeferenced data points with GPR-derived ice thicknesses, in addition to a glacier boundary line derived from satellite images taken during summer, were interpolated over the entire glacier surface using kriging with a 10 m grid size. Some uncertainty analysis were carried on and we calculated an averaged ice thickness of 76 m and a maximum depth of 164 m with a relative error of 11.9%. The volume of the glacier is derived as 0.3487 ± 0.041 km^3. Finally a 10-m grid map of the bedrock topography was derived by subtracting the ice thicknesses from a dual-frequency GPS-derived digital elevation model of the surface. These two datasets are the first step for modelling thermal evolution of the glacier and its bedrock, as well as the main hydrological network.

Keywords: Glacier; Ground-penetrating Radar; Ice Volume Estimation

I. INTRODUCTION

Long-term studies of the Spitsbergen Western coast glaciers reveal that they are retreating over the last decades (Hagen et al., 2003; Kohler et al., 2007). Quantification of current mass-balance trends of these glaciers is attempted by the evaluation of surface conditions (accumulation and ablation), basal conditions (melting or freezing) and ice dynamics (mass movements). Surface changes can be evaluated from digital elevation models (DEMs) derived, e.g. from photogrametric methods applied on aerial and satellite images, surface GPS measurements or airborne LiDAR acquisitions or ground based high resolution photography (Cuffey and Paterson, 2010; Bernard et al., in press) in addition to *in situ* ablation stake network height measurements. However, the glacier volume estimate is necessary for either ice dynamical modelling or future mass balance scenarios.

Ground-penetrating Radar (GPR) is a geophysical tool using radiofrequency electromagnetic waves for sounding underground features. This method is especially efficient for mapping glaciers thanks to the good penetration depth of the electromagnetic waves in a low loss medium such as ice. Common-offset radar profiling has been successfully used for evaluating ice thickness of glaciers (e.g. (Hagen and Sætrang, 1991; Ramírez et al., 2001; Fischer, 2009)), deriving at a decimetric scale the internal geometry of ice structures (Hambrey et al., 2005), locating and characterizing englacial channels (Stuart et al., 2003) and analyzing the glacier base for determining the thermal regime (Murray et al., 2000; Murray and Booth, 2009). Multi-offset profiles are acquired for getting a wave velocity estimate or the water content variations of the glacier ice (Murray et al., 2007). It is striking to see the evolution in the radar surveys since the 1990s when measurement positioning was achieved using compass and visual navigation on the glacier and the main source of error in the ice thickness estimation was considered to be $\pm$ 10 m mostly due to the digitizing of the profiles (Hagen and Sætrang, 1991). High resolution, real time positioning capability as provided by GNSS and, in our case, GPS, provides the mandatory tool for high resolution bedrock mapping on challenging terrain.

The Austre Lovénbreen is a northward-flowing valley glacier situated in the Brøgger peninsula, Spitsbergen, Norway (79^{o}N) (Mingxing et al., 2010; Bernard, 2011). It extends from an altitude of 100 m to 560 m above sea level. The mean annual precipitation is 391 mm and its mean annual temperature from 1969 to 1998 is -5.77^{o}C (source DNMI at http://eklima.met.no). Thanks to the geological configuration of its basin, all runoff water is concentrated into two channels. With this specific hydrological configuration and being near the former mining town of Ny-Ålesund, this site has been the focus of intense scrutiny since the 1960s. A summary of historical dataset since 1962, used for elevation models on this glacier as well as their relevance to evaluate mass balance is described in (Friedt et al., 2012). The neighboring glacier, Midtre Lovénbreen, has been extensively studied as well. It is known to be polythermal on the basis of radio echo sounding (Hagen and Sætrang, 1991; Björnsson et al., 1996; Rippin et al., 2003). A detailed description of its structure and dynamics can be found in (Hambrey et al., 2005). Additionally to a high frequency GPR survey, a seismic reflection survey allowed for determining the properties of the bed material (King et al., 2008).

In this paper we present results of a high density coverage GPR survey (120 profiles resulting in 67542 ice thickness measurements) of the Austre Lovénbreen. We first show some internal structures observed on selected radargrams, then present the ice volume estimation and finally the glacier substratum topography. We discuss

the different sources of uncertainties in those two data sets.

II. Data collection and processing

We used a Malå Ramac GPR operating at 50 and 100 MHz to collect more than 70 km of mono-offset profiles (Fig. 1) over the surface of the Austre Lovénbreen (Svalbard) during 3 weeks in April 2010. Both the 50 MHz and 100 MHz antenna data, corresponding to a nominal wavelength in ice of 3.4 m and 1.7 m respectively, were collected in the form of 2806 samples within a time window 2.224 μs. All data were stacked 8 times on collection. Positioning of all GPR mono-offset profiles was done using a Globalsat ET-312 Coarse/Acquisition (C/A) code GPS receiver connected to the control unit of the GPR, set to 1 measurement per second while two operators were pulling the device at a comfortable walking pace. A trace was acquired every 0.5 s, and the average distance between traces was later calculated at 0.3 m.

[Fig. 1 about here.]

Snow cover was evaluated through 42 snow drilling measurements regularly spaced to cover all the glacier. These data were acquired at the time of the GPR and dual GPS measurements and subsequently interpolated using ordinary kriging. The resulting snow thickness map is shown on Fig. 2. The measurement root mean square error is 20 cm (Webster and Oliver, 2001). The average snow thickness over the entire glacier on April 2010 was estimated to 1.67 m.

[Fig. 2 about here.]

In addition to the mono-offset profiles, one Common Mid-Point (CMP) gather was acquired on the glacier snout using the 100 MHz antennas (Fig 3). The initial separation between antennas was 0.5 m, with a spatial stepsize of 0.5 m. CMP data were interpreted using coherence analysis, defined equivalently to semblance but using an analysis window of one temporal sample (here, 0.8 ns). The basal reflection exhibits a velocity of 0.1715 m/ns (red trajectory in CMP gather, lower pick in coherence panel), but coherence delivers a root-mean-square velocity that is biased systematically slow with respect to its true value (Booth et al., 2010). This occurs because true velocity is only expressed by wavelet first-breaks, yet these are zero amplitude hence cannot produce a coherence response. We therefore use the coherence response to simulate first-break travel-times, using the 'backshifting' method of Booth et al. (2010), and obtain an RMS velocity of 0.1747 m/ns and a travel-time to the base of the ice of 140.0 ns (blue trajectory in CMP gather, upper pick in coherence panel).

This RMS velocity is then converted to interval velocity using Dix's equation (Dix, 1955). At the location of the CMP acquisition, the glacier was covered by 0.7 m of snow, which we assume to have a velocity of 0.22 m/ns (Murray et al., 2007) and, hence, the two-way travel-time to the base of the snow is 6.3 ns. Substituting our velocity-time model into Dix's Equation gives 0.1723 ± 0.0021 m/ns as the interval velocity through the ice, and a local ice thickness of 10.21 ± 0.16 m. The uncertainty in these values is obtained by considering the resolution of coherence analysis (Booth et al., 2011), and is therefore representative of the error between a given coherence pick and its true velocity value.

Successive depth conversions are made with a velocity value of 0.17 m/ns, which represents the lower-bound of the error in interval velocity. We choose this value since the volumetric content of air is likely to decrease

in the thicker parts of the glacier (Gusmeroli et al., 2010) hence we anticipate that a slower velocity is more widely representative. Although CMP surveys over the thickest ice could confirm this, the fiber optic cables of our GPR system were only 20 m long, reducing our maximum offset-to-depth ratio and thereby producing a poor coherence response. Finally, we will use the velocity derived from the 100 MHz dataset to depth-convert 50 MHz records. Ice is weakly dispersive: across the range 1-100 MHz, relative dielectric permittivity decreases by 0.04 (Dowdswell and Evans, 2004). Accordingly, in terms of propagation velocity, if our 100 MHz wavelet travels at 0.1700 m/ns, a 50 MHz wavelet travels at 0.1695 m/ns, a difference that we consider negligible in depth conversion.

[Fig. 3 about here.]

Mono-offset GPR data have been processed using Seismic Unix software (Cohen and Stockwell, 2011; Stockwell, 1999). A residual median filter was applied in vertical direction using a time window corresponding to the cut-off frequency of 50 MHz, each trace has been normalized to its root mean square value and bandpass filtered. Each profile was chopped above the arrival time of the minimum amplitude of the direct air wave (manually selected). Based on the ET312 C/A GPS information, the mean distance a between traces is computed. Equidistant trace positioning is achieved by searching for the acquired trace located closest to a periodic grid of period a. The obtained profiles have then been migrated using a Stolt algorithm with a velocity of 0.17 m/ns. When needed for visualization, elevation correction was implemented using the altitude given by the ET312 C/A GPS.

During the GPR survey, a dense elevation map was performed using GPS measurements with a snowmobile: a Trimble Geo-XH dual frequency receiver, with electromagnetic delay correction post-processing using the nearby ($<$10 km away) Ny-Ålesund reference dataset, provided the raw data to generate a DEM of the glacier after interpolation of the dataset. Data processing is performed in two steps. First the ice thickness is derived from GPR profiles, with removal of the snow thickness contribution. In a second step, the bedrock surface is interpolated and located in space by subtracting the ice thickness from the surface DEM.

III. Glacier structures

For giving an insight on our GPR data quality, four processed radargrams are shown on Fig. 4, 5, **??** and 7. AA' was acquired along the glacier central axis toward North while BB' was acquired from West to East across the glacier (see Fig. 1). CC' was acquired across the glacier tongue.

[Fig. 4 about here.]

[Fig. 5 about here.]

[Fig. 6 about here.]

Along AA', the strong continuous reflection is interpreted as the ice–bedrock interface. The main ice-flow direction is South to North (Mingxing et al., 2010). At the beginning of the profile, multiple scattering occurs partially masking the ice–bedrock interface, preventing sometime the picking of the arrival time of the radar reflection on this interface. Similar zones are observed only on the western upper side of the glacier as in profile

BB' beginning. We interpret these as reflections on fallen rocks incorporated into the ice, or infiltrated water. Around 700 m, the bedrock topography rises by 50 m over a distance of 200 m creating a local topographical high. This feature may be related to the geology of the area: a thrust fault between the Welderyggen thrust sheet and the Nielsenfjellet thrust sheet is indicated in the southern part of the Lovénbreen glacier in geological maps (Hjelle, 1993; Saalmann and Thiedig, 2002). Heading farther north the bedrock surface is easy to follow all the way down to the glacier frontal moraine. At 3000 m along this profile, the ice thickness decreases as the bedrock topography rises 70 m. The same trends are observed in other parallel profiles.

[Fig. 7 about here.]

On BB' radargram, the bedrock reflection is very clear except in two areas. In the middle part of the glacier (around 1300 m), an area with increased scattering appears in the deepest part of the glacier, and we attribute this to the presence of temperate ice as described in the neighboring glacier (Hagen and Sætrang, 1991; Moore et al., 1999; King et al., 2008). This multiple scattering area prevented us from picking the ice–bedrock interface reflection resulting into a gap in ice thickness estimates as visible on Fig. 1. In this figure, other gaps in the center part of the glacier result from the same difficulty to pick the ice–bedrock interface due to high scattering zones, giving thus an idea of the horizontal extension of the probable temperate ice.

On the first 500 m of BB', many scatterers are again observed, associated with either fallen rocks or infiltrated water given the proximity to the surrounding mountain side. The bedrock reflection disappears among all the scatterers but it becomes detectable in the profile acquired in this area using 50 MHz antenna (Fig. 6). This 50 MHz migrated profile was used to pick the ice–bedrock interface instead of the first 900 m of profile BB'. At 1000 m along the profile, 30 m deep, some large hyperbolae are attributed to buried englacial channels. Our data set does not present parallel profiles close enough to BB' to determine the horizontal extension of this channel.

Fig. 7 shows one processed profile across the glacier tongue along the profile CC' of Fig. 1. This profile crosses a buried supraglacial stream, evident on the satellite image of June 26th 2007, copyright FORMOSAT. Where this stream intersects CC', at around 800 m, the radargram shows many diffraction hyperbolae. This feature can be observed an all radargrams that cross the stream.

IV. Ice volume estimation

The boundary of the glacier (grey line in Fig. 1), 14143 m long, was drawn on a summer 2009 FORMOSAT image. Whenever visible, rimaye (bergschrunds) were considered as the limit between the glacier and slopes. Moreover, slope angles were derived and used to differentiate steep angle slopes and low angle glacier. Field knowledge and direct local GPS measurements were of great help as well. Visual inspection of all these elements allowed us to determine as precisely as possible the limits of the glacier. We estimate that the glacier boundary is identified with a ± 10 m uncertainty. The area of the glacier is thus measured to be 4.6 ± 0.28 km^2. We have decided to define a null ice thickness on the boundary. We will see that this choice will not significantly affect the ice volume estimate: assuming a maximum of 20 m ice thickness error along this boundary, the volume contribution is 0.0056 km^3 (1.6% relative error).

In every migrated GPR profile, the arrival time of the basal reflection was picked using Reflexw software (Sandmeier, 2007). No picking was done where the ice–bedrock interface was not clear. The two-way travel time is translated into ice thickness using 0.17 m/ns velocity as derived earlier from CMP analysis: the uncertainty on this velocity contributes to 1.2 % uncertainty on the glacier volume (Fig. 9). The snow layer contribution (Fig. 2) to the radar wave propagation duration is removed by subtracting its corresponding time delay assuming a velocity of 0.22 m/ns. The uncertainty on the snow thickness of 20 cm contributes to a volume of 9.2×10^{-4} km^3 (0.3% relative error).

The analysis ended-up with a total of 67542 georeferenced data points with GPR-derived ice thickness. All ice-thickness measurements were interpolated over the entire glacier surface using a kriging method onto a 10 m grid (Fig. 9). The ice volume is 0.3487 km^3. Notice that working on non migrated data as in (Saintenoy et al., 2011) yields a volume of 0.3427 km^3, or a 1.1 % error with respect to the volume derived from migrated data.

[Fig. 8 about here.]

Depth estimate quality assessment was performed by analyzing the error between ice-thickness estimates from closely-separated traces in distinct profiles: the thickness difference between the closest points lying less than 3 m apart was computed and the histogram of the ice-thickness distribution is plotted (Fig. 8). A gaussian fit of each histogram is performed using a constrained nonlinear optimization method: we analyze the whole dataset including all traces intersections (blue dots) and separately the particular case of five transects acquired 3 to 5 days apart but following the same path (snow tracks). This latter case seems relevant of errors due solely to the analysis of the migrated data and not to reflections of the electromagnetic wave along different interfaces due to different antenna orientations at a given intersection point. The global histogram exhibits a standard deviation of 0.51 m and a negligible mean value of -0.17 m. These results, suggesting a better agreement than other analysis found in the literature (Fischer, 2009; Hagen and Sætrang, 1991), is however optimistic by including the five repeated transects with standard deviation 0.46 m and mean value of -0.18 m. Using only intersections of traces crossing at high angles by excluding the five repeated transects (Fig. 8, top, red points), the standard deviation of the histogram increases to 1.77 m with a mean value of 0.37 m. This histogram of the ice thickness differences at intersections analysis is consistent with the result of the surface interpolation by kriging, which provides an estimate of the root-mean square error between experimental data and the interpolated surface of 0.7 m. The interpolation of ice thickness outside of the tracks yields the largest source of uncertainty, as provided by the kriging prediction standard error map shown on Fig. 10, with a 11.5% contribution to the ice volume calculation (corresponding to an average error of 8.72 m on the interpolated ice thickness).

As a result, the ice volume was estimated to 0.3487 $\pm$ 0.041 km^3, with all contributions to the uncertainty summarized in Table I. This result is to be compared with the empirical formula found in (Hagen et al., 1993) for outlet glaciers whose area A exceeds 1 km^2: the mean depth is estimated as $D = 33\log(A) + 25$. In our case, $A = 4.6 \pm 0.28$ km^2 yields a mean depth of 75$\pm$2 m, surprisingly close to the 76 m we found from our analysis.

[TABLE 1 about here.]

V. Bedrock digital elevation model

The Coarse/Acquisition (C/A) code GPS receiver that was used when GPR data was acquired is in the range of a 3 m standard deviation in latitude and longitude but displays an unacceptable vertical accuracy with respect to the DEM resolution. Therefore, only dual-frequency acquired GPS altitude measurements were used as DEM reference for bedrock positioning. The accuracy of surface DEM is discussed in detail in Friedt et al. (2012). The same uncertainty analysis carried on the dual-frequency GPS measurements yields an altitude distribution with a standard deviation less than 0.6 m. Thus, considering a 11.9 % error on the 76 m-mean depth glacier thickness (or 9 m) and a 0.6 m standard deviation on the DEM height, the bedrock topography uncertainty (standard deviation of altitude error) is 9.6 m over the measurement points. The error analysis from the kriging interpolation rises this error on the interpolated areas to 19 m for areas far from any experimental dataset (cf Fig. 10).

[Fig. 9 about here.]

[Fig. 10 about here.]

[Fig. 11 about here.]

Figs. 9 and 11 show the asymmetry of the bedrock underneath the ice on the glacier snout. The substratum is deeper on the easter side of the glacier. Furthermore, the ice–bedrock appears convex (bulging outward) on the western side and concave (hollowed inward) on the eastern side as seen on the GPR profiles acquired across the glacier snout (Fig. 7). This observation is consistent with a difference in the hardness of the underlying rock, and possibly to the transform fault presented in the geological map of Saalmann and Thiedig (2002) in between the Slatto and the Haavimb summits (Fig. 11).

VI. Conclusion

A high resolution mapping by 100-MHz and 50-MHz GPR of a polar glacier provides a detailed bedrock topography information. While the average ice thickness of 76 m is consistent with empirical data derived from glaciers in the Svalbard area, the high resolution dataset obtained by walking yields a rich information including subsurface structures (crevasse fields, bedieres, supraglacial stream) and ice volume distribution amongst the various glacier substructures (cirques). The resulting volume is estimated to 0.3487 ± 0.047 km^3, with the main source of error being the interpolation uncertainty of the ice thickness between tracks.

Such volume distribution provide the basic input for further mass balance investigations. Furthermore, high density GPR data coverage coupled to accurate DEM obtained by dual frequency GPS provides a map of the bedrock following an interpolation by kriging. This bedrock digital elevation model exhibits asymmetric features consistent with geological structures (faults) in the area. Bedrock morphology can now be used to investigate subglacial water flow paths, to be improved by considering the influence of ice pressure.

ACKNOWLEDGMENT

This program was funded by the ANR program blanc-0310, the IPEV program 304 and the CNRS-GDR 3062 Mutations polaires. Adam Booth is supported by the Leverhulme-funded GLIMPSE project. The authors would like to thank AWIPEV for the logistical support in Ny-Ålesund, Tavi Murray for her much helpful comments to realize this work, Nerouz Boubaki and Emmanuel Léger for picking some GPR data and Mélanie Quenet for pointing out some references on the geology of the area.

VII. References

Bernard, E., Friedt, J.-M., Tolle, F., Griselin, M., Martin, G., Laffly, D., and Marlin, C., in press, Monitoring seasonal snow dynamics using ground based high resolution photography (Austre Lovénbreen, Svalbard, 79^o N): ISPRS Journal of Photogrammetry and Remote Sensing.

Bernard, E., 2011, Les dynamiques spatio-temporelles d'un petit hydrosystème arctique : approche nivo-glaciologique dans un contexte de changement climatique contemporain (bassin du glacier Austre Lovénbreen, Spitsberg, 79 ^{o} N): Ph.D. thesis, Université de Franche-Comté, Besançon.

Björnsson, H., Gjessing, Y., Hamran, S., Ove Hagen, J., Liestøl, O., Pálsson, F., and Erlingsson, B., 1996, The thermal regime of sub-polar glaciers mapped by multi-frequency radio-echo sounding: Journal of Glaciology, **42**, 23–32.

Booth, A. D., Clark, R., and Murray, T., 2010, Semblance response to a ground-penetrating radar wavelet and resulting errors in velocity analysis: Near Surface Geophysics, **8**, no. 3, 235–246.

Booth, A. D., Clark, R., and Murray, T., 2011, Influences on the resolution of GPR velocity analyses and a Monte Carlo simulation for establishing velocity precision: Near Surface Geophysics, **9**, no. 5, 399–411.

Cohen, J., and Stockwell, J. CWP/SU: Seismic Un*x Release No. 42: an open source software package for seismic research and processing:. www.cwp.mines.edu/cwpcodes, 2011.

Cuffey, K. M., and Paterson, W. S. B., 2010, The Physics of Glaciers: Boston, Elsevier, fourth edition.

Dix, C. H., 1955, Seismic velocities from surface measurements: Geophysics.

Dowdswell, J. A., and Evans, S., 2004, Investigations of the form and flow of ice sheets and glaciers using radio-echo sounding: Reports on Progreess in Physics, 1821–1861.

Fischer, A., 2009, Calculation of glacier volume from sparse ice-thickness data, applied to Schaufelferner, Austria: Journal of Glaciology, **55**, no. 191, 453–460.

Friedt, J.-M., Tolle, F., Bernard, E., Griselin, M., Laffly, D., and Marlin, C., 2012, Assessing the relevance of digital elevation models to evaluate glacier mass balance: application to Austre Lovénbreen (Spitsbergen, 79^{o}N): Polar Record, **48**, no. 244, 2–10.

Gusmeroli, A., Murray, T., Jansson, P., Pettersson, R., Aschwanden, A., and Booth, A. D., 2010, Vertical distribution of water within the polythermal Storglaciaren, Sweden: Journal of Geophysical Research, **115**, F04002.

Hagen, J. O., and Sætrang, A., 1991, Radio-echo soundings of sub-polar glaciers with low-frequency radar: Polar Research, **9**, no. 1, 99–107.

Hagen, J. O., Liestøl, O., Roland, E., and Jørgensen, T., 1993, Glacier Atlas of Svalbard and Jan Mayen: Norsk Polarinstitutt.

Hagen, J. O., Kohler, J., Melvold, K., and Winther, J.-G., 2003, Glaciers in Svalbard: mass balance, runoff and freshwater flux: Polar Research, **22**, 145–159.

Hambrey, M. J., Murray, T., Glasser, N. F., Hubbard, A., Hubbard, B., Stuart, G., Hansen, S., and Kohler, J., 2005, Structure and changing dynamics of a polythermal valley glacier on a centennial timescale: Midre Lovénbreen, Svalbard: Journal of Geophysical Research (Earth Surface), **110**, 1006–+.

Hjelle, A., 1993, Geology of Svalbard:, volume 7 Oslo: Norsk Polar Institute.

King, E. C., Smith, A. M., Murray, T., and Stuart, G. W., 2008, Glacier-bed characteristics of Midtre Lovénbreen, Svalbard, from high-resolution seismic and radar surveying: Journal of Glaciology, **54**, 145–156.

Kohler, J., James, T. D., Murray, T., Nuth, C., Brandt, O., Barrand, N. E., Aas, H. F., and Luckman, A., 2007, Acceleration in thinning rate on Western Svalbard glaciers: Geophysical Research Letters, **34**, 1–5.

Mingxing, X., Ming, Y., Jiawen, R., Songtao, A., Jiancheng, K., and Dongchen, E., 2010, Surface mass balance and ice flow of the glaciers Austre Lovénbreen and Pedersenbreen, Svalbard, Arctic: Chine Journal of Polar Science, **21**, no. 2, 147–159.

Moore, J. C., Palli, A., Ludwig, F., Blatter, H., Jania, J., Gadek, B., Glowacki, P., Mochnacki, D., and Isaksson, E., 1999, High-resolution hydrothermal structure of Hansbreen, Spitsbergen, mapped by ground-penetrating radar: Journal of Glaciology.

Murray, T., and Booth, A. D., 2009, Imaging glacial sediment inclusions in 3-D using ground-penetrating radar at Kongsvegen, Svalbard: Journal of Quaternary Science, **25**, no. 5, 754–761.

Murray, T., Stuart, G. W., Miller, P. J., Woodward, J., Smith, A. M., Porter, P. R., and Jiskoot, H., 2000, Glacier surge propagation by thermal evolution at the bed: Journal of Geophysical Research.

Murray, T., Booth, A., and Rippin, D. M., 2007, Water-content of glacier-ice: Limitations on estimates from velocity analysis of surface ground-penetrating radar surveys: Journal of Environmental and Engineering Geophysics, **12**, no. 1, 87–99.

Ramírez, E., Francou, B., Ribstein, P., Descloitres, M., Guerin, R., Mendoza, J., Gallaire, R., Pouyaud, B., and Jordan, E., 2001, Small glaciers disappearing in the tropical Andes: a case-study in Bolivia: Glaciar Chacaltaya (16° S): Journal of Glaciology, **47**, no. 157, 187–194.

Rippin, D., Willis, I., Arnold, N., Hodson, A., Moore, J., Kohler, J., and Björnsson, H., 2003, Changes in geometry and subglacial drainage of Midre Lovénbreen, Svalbard, determined from digital elevation models: Earth Surface Processes and Landforms, **28**, no. 3, 273–298.

Saalmann, K., and Thiedig, F., 2002, Thrust tectonics on Broggerhalvoya and their relationship to the Tertiary West Spitsbergen Fold-and-Thrust Belt: Geol. Mag., **139**, 47–72.

Saintenoy, A., Friedt, J.-M., Tolle, F., Bernard, E., Laffly, D., Marlin, C., and Griselin, M., June 2011, High density coverage investigation of the Austre Lovénbreen (Svalbard) using ground-penetrating radar: 6th International Workshop on Advanced Ground Penetrating Radar (IWAGPR).

Sandmeier, K. J. **Reflexw manual, version 4.5**. www.sandmeier-geo.de, July 2007.

Stockwell, J. W., May 1999, The CWP/SU: Seismic Un*x Package: Computers and Geosciences, pages 415–419.

Stuart, G., Murray, T., Gamble, N., Hayes, K., and Hodson, H., 2003, Characterization of englacial channels by ground-penetrating radar: An example from Austre Brøggerbreen, Svalbard: Journal of Geophysical Research, **108**, no. B11, 2525–+.

Webster, R., and Oliver, M. A., 2001, Geostatistics for environmental scientists (Statistics in Practice): John Wiley and Sons, Brisbane, Australia, 1^{st} edition.

LIST OF FIGURES

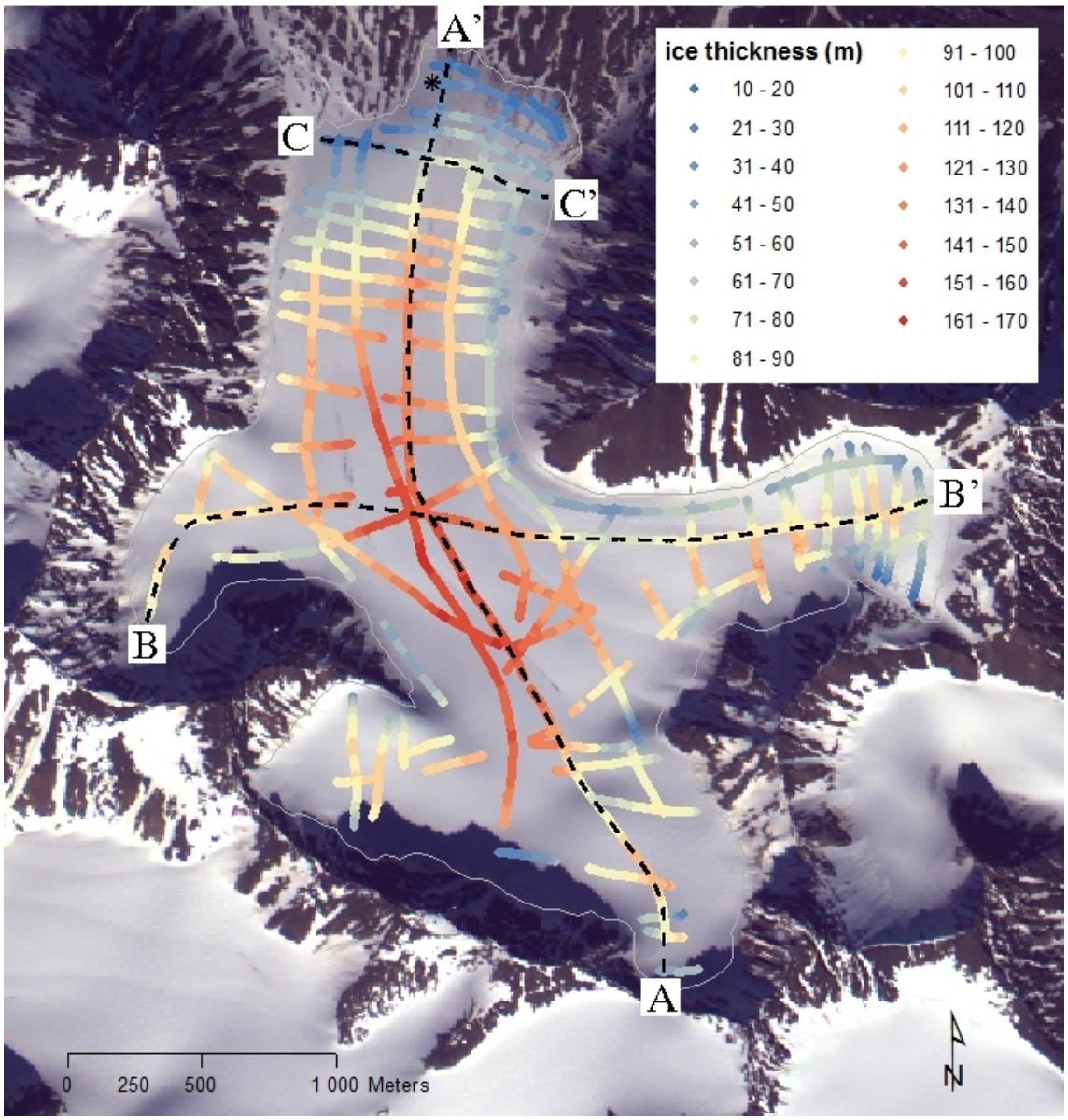

Fig. 1. GPR profiles over the Austre Lovénbreen (background image copyright FORMOSAT). The color scale indicates the ice thickness measured on each profiles. Dashed lines indicate GPR transects displayed on Fig. 4 to 7. The symbol $*$ indicates the CMP position.

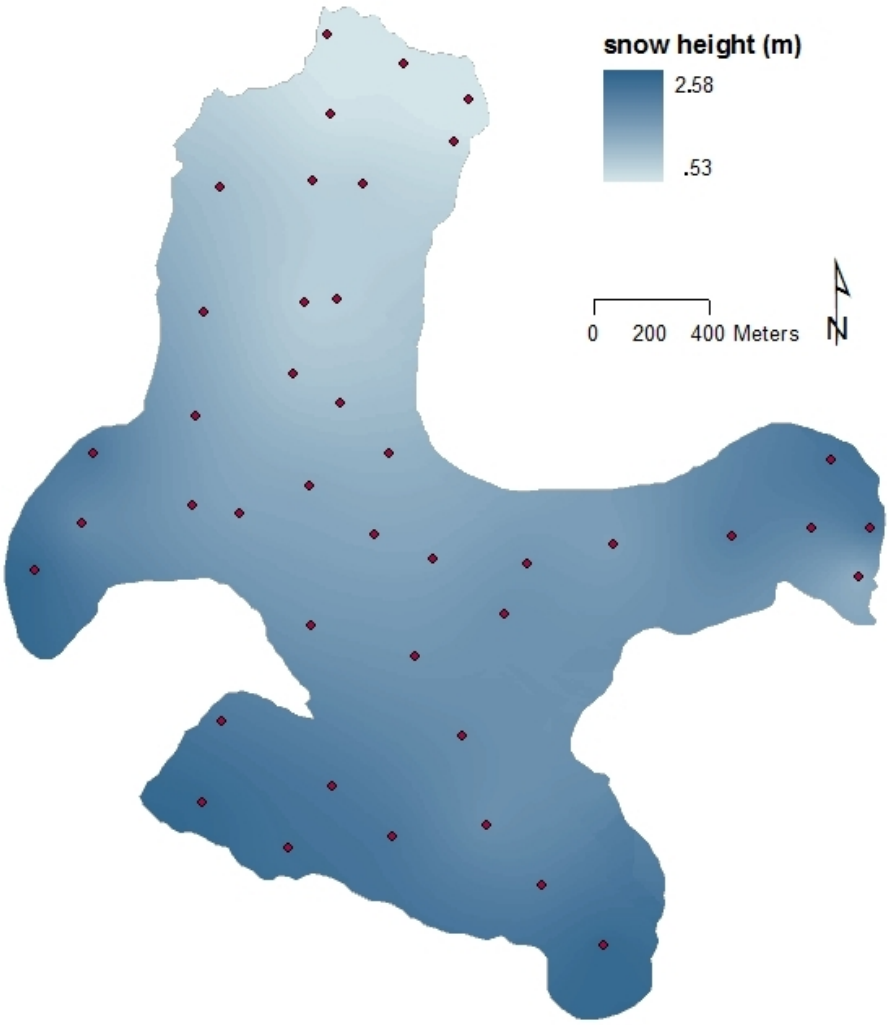

Fig. 2. Snow thickness map interpolated from 42 snow drilling measurements indicated by the red dots. The mean snow thickness was evaluated to 1.67 m.

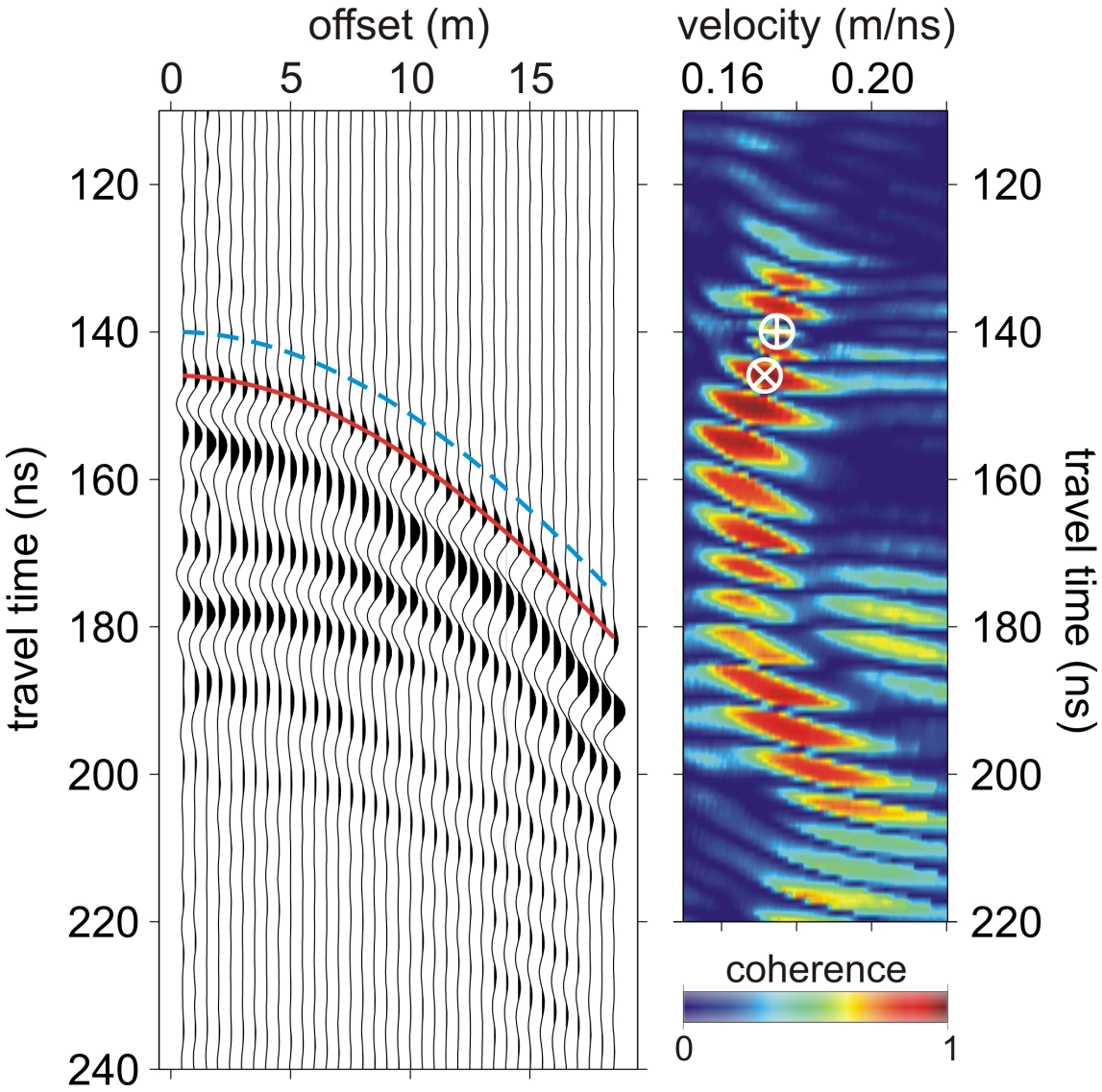

Fig. 3. Coherence analysis of CMP data located on the glacier snout (Fig. 1). Left: CMP data and reflection trajectories, as defined from coherence analysis (right). The lower hyperbola (red) corresponds to the lower coherence pick, and is interpreted as the reflection from the ice–bedrock interface. After application of backshifting (Booth et al., 2010), we define the upper hyperbola (blue, dashed) and coherence pick as a better approximation to first-break travel-times.

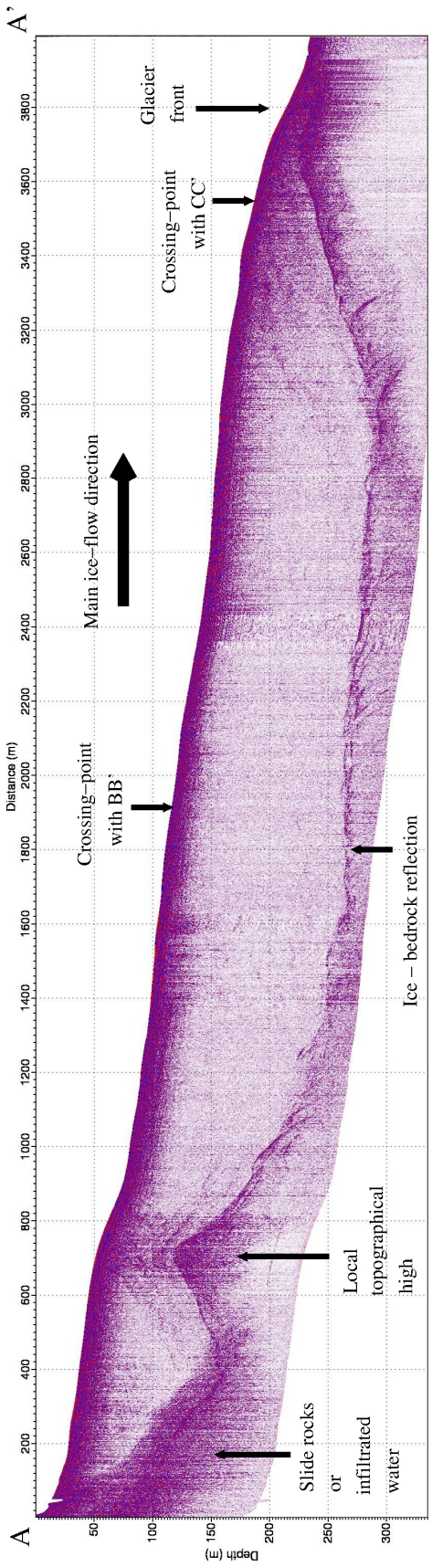

Fig. 4. Radargram AA' acquired along the glacier axis with 100 MHz antennas including topography corrections.

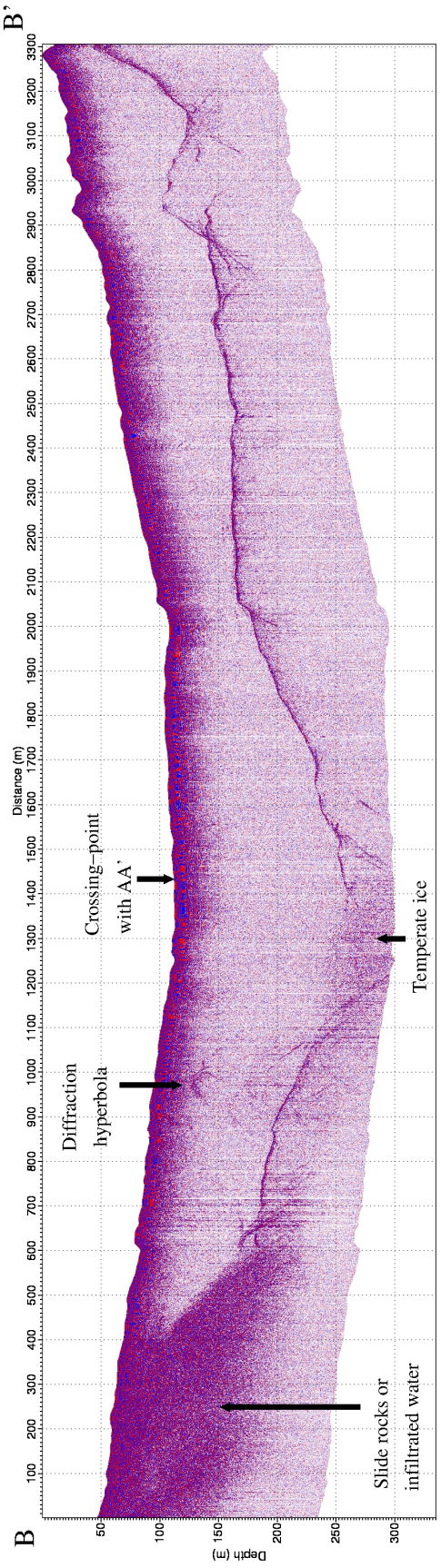

Fig. 5. Radargram BB' acquired across the glacier axis with 100 MHz antennas (non migrated).

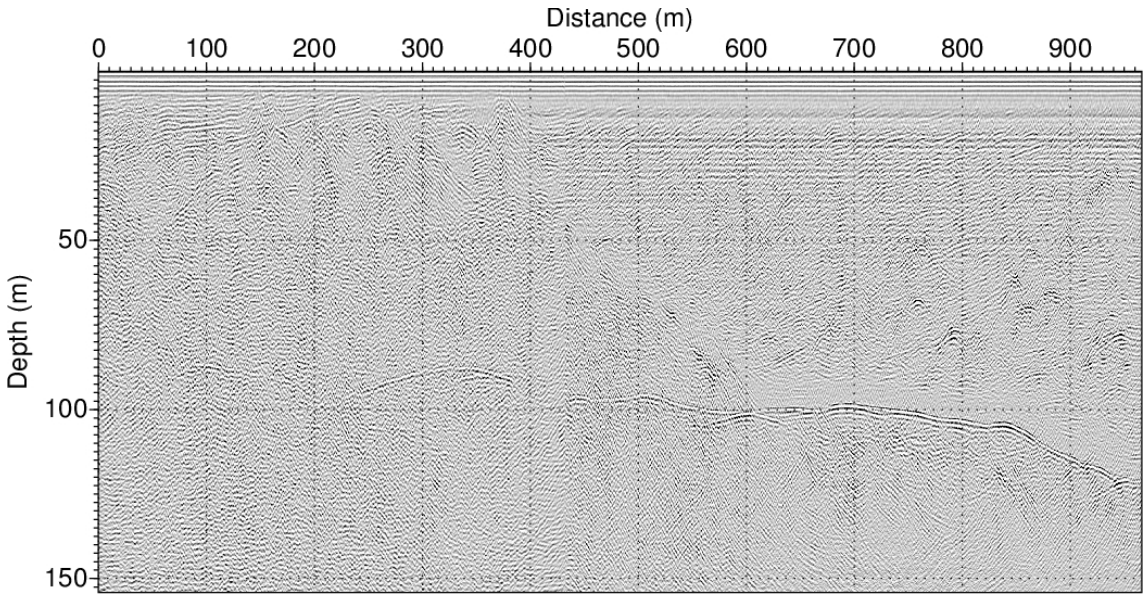

Fig. 6. Repetition of the first 900 m of profile BB' with 50 MHz antennas (after Stolt migration using a velocity of 0.17 m/ns, with AGC gain but no topographic corrections).

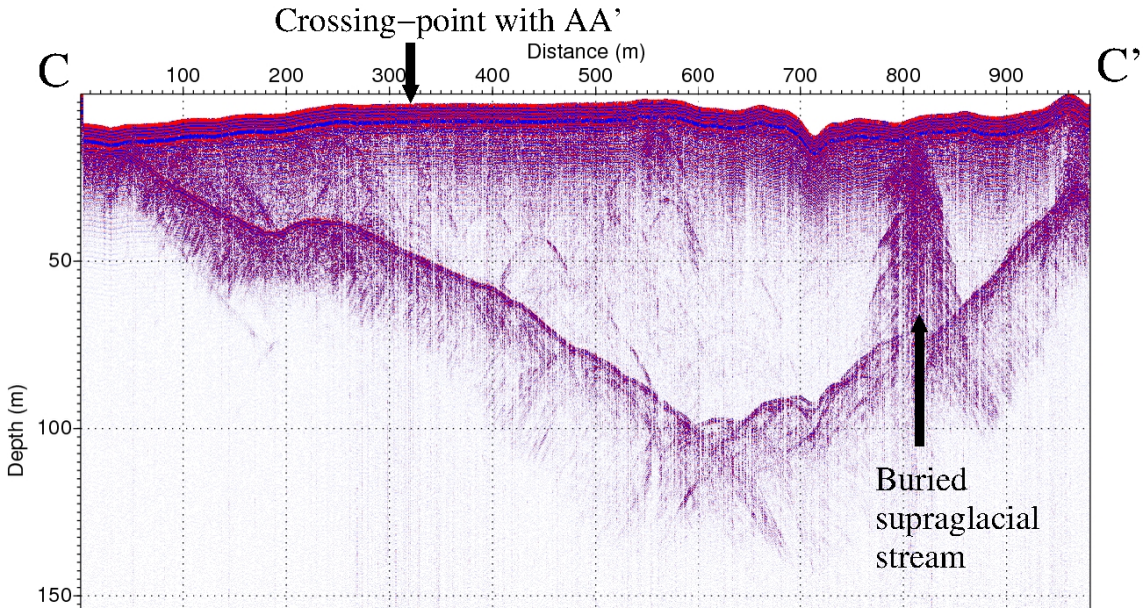

Fig. 7. Radargram CC’ acquired across the glacier tongue with 100 MHz antennas (non migrated).

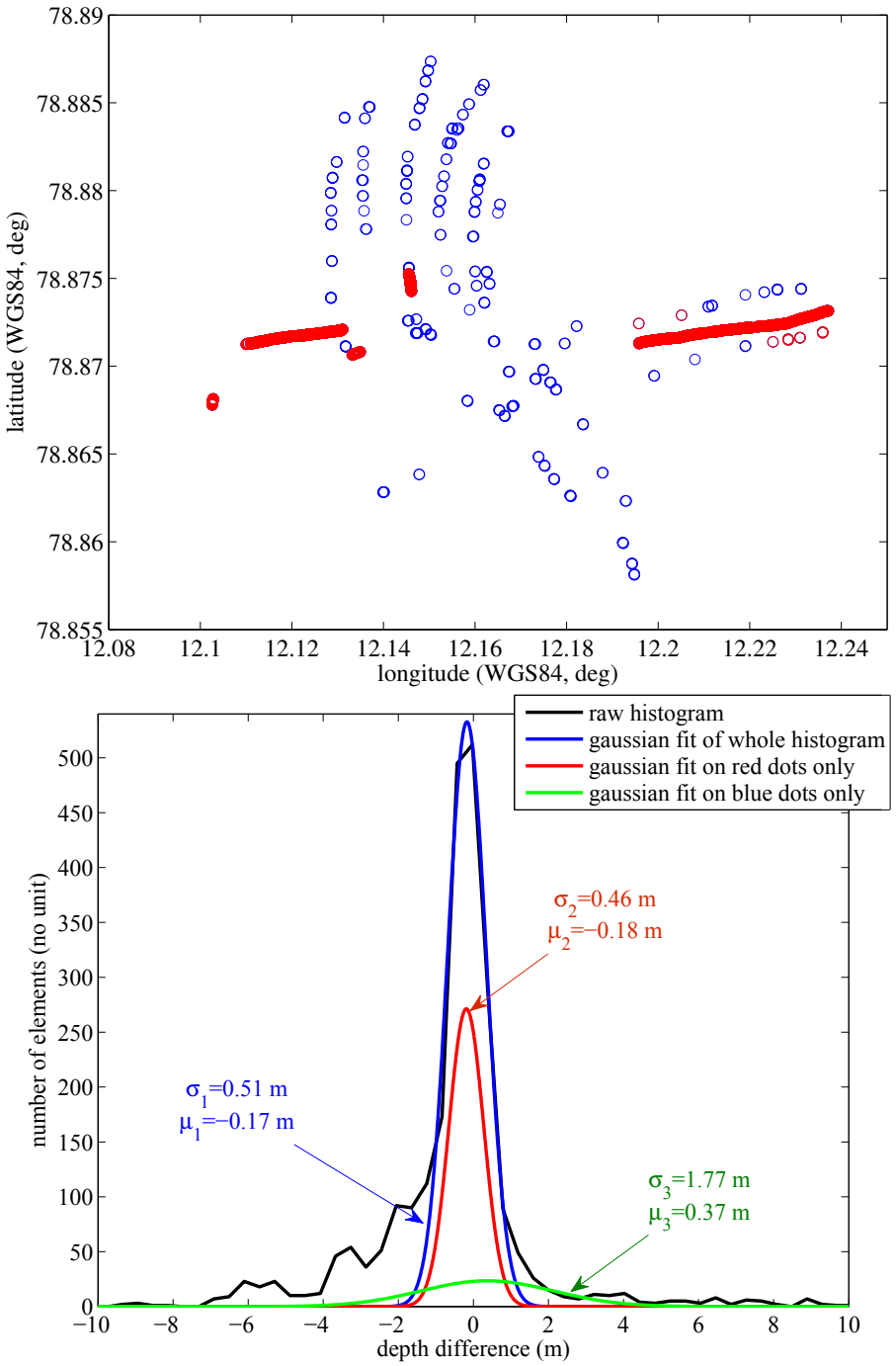

Fig. 8. Top: map of the analyzed intersection points with *closest points located less than 3 m from each other at each GPR track intersection. Blue is all intersection points, red is a particular case of two measurements performed several days apart but following the exact same path over the glacier (tracks left in the snow). Bottom: histogram of the depth difference distribution. The analysis was performed on various subsets of the intersection dataset, with the standard deviation σ and the mean value μ of the gaussian fit indicated for each contribution.*

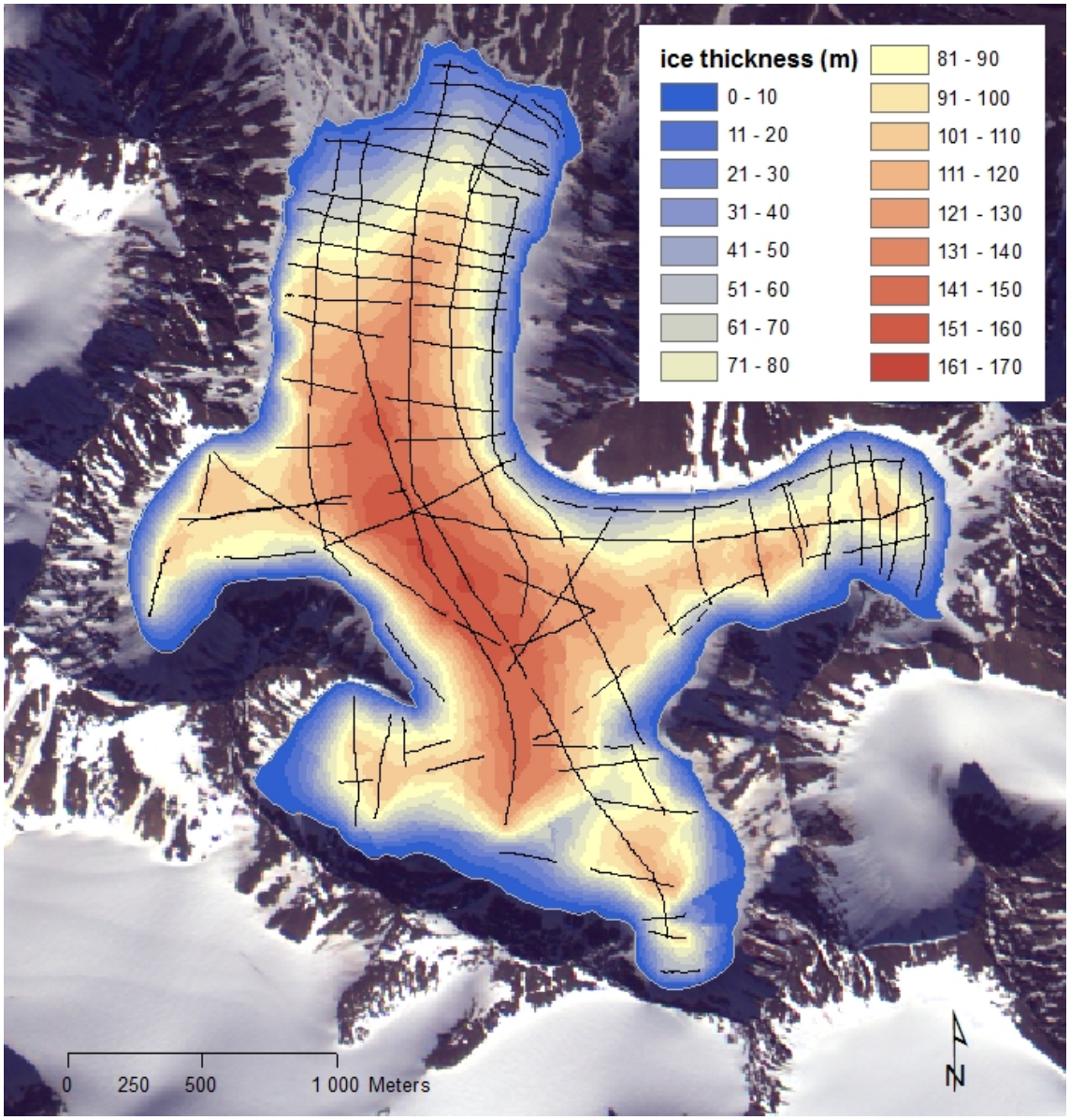

Fig. 9. Interpolated ice thickness with GPR transects in black lines (background image copyright FORMOSAT).

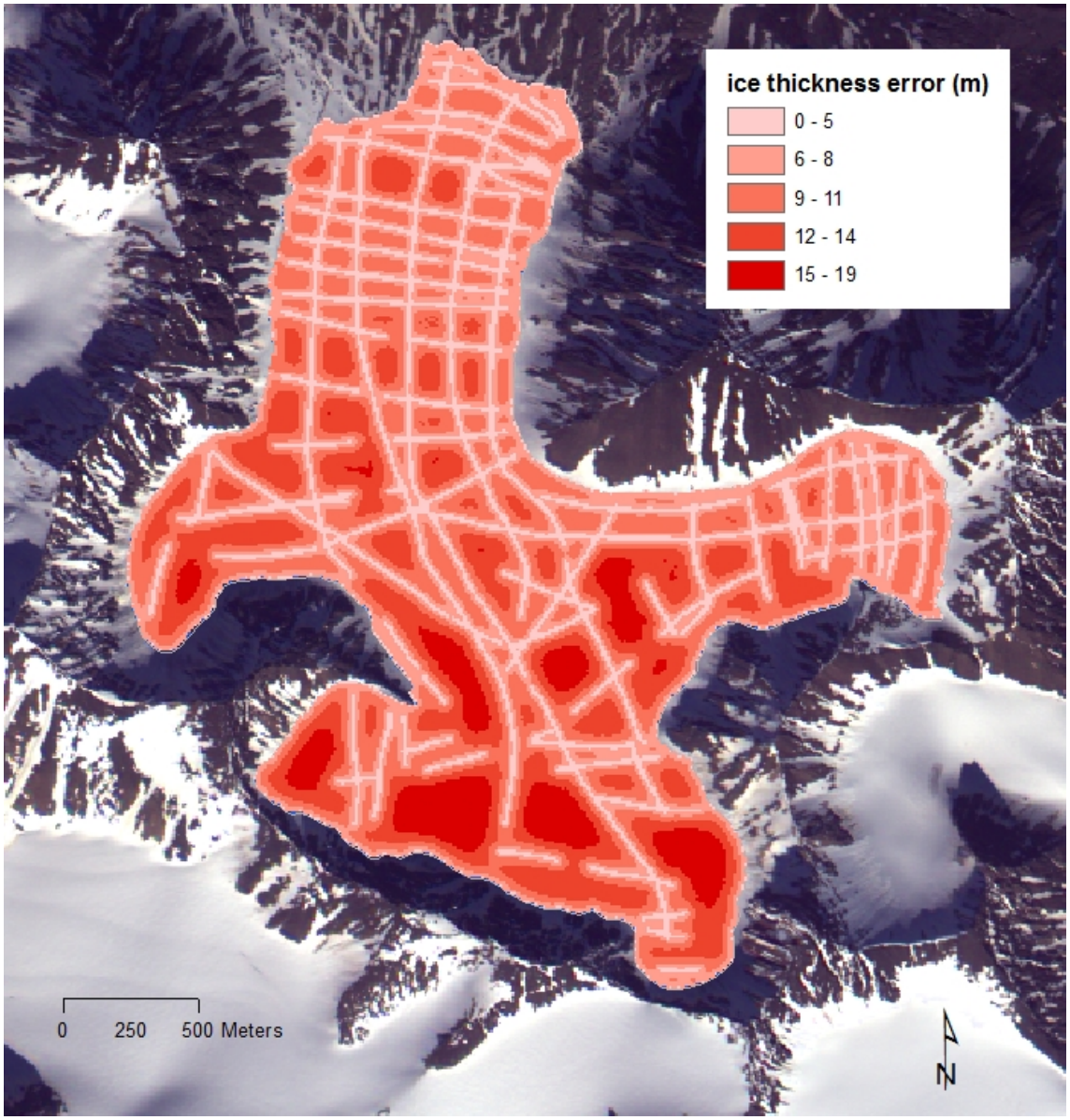

Fig. 10. Prediction standard error map of interpolated ice thicknesses (background image copyright FORMOSAT).

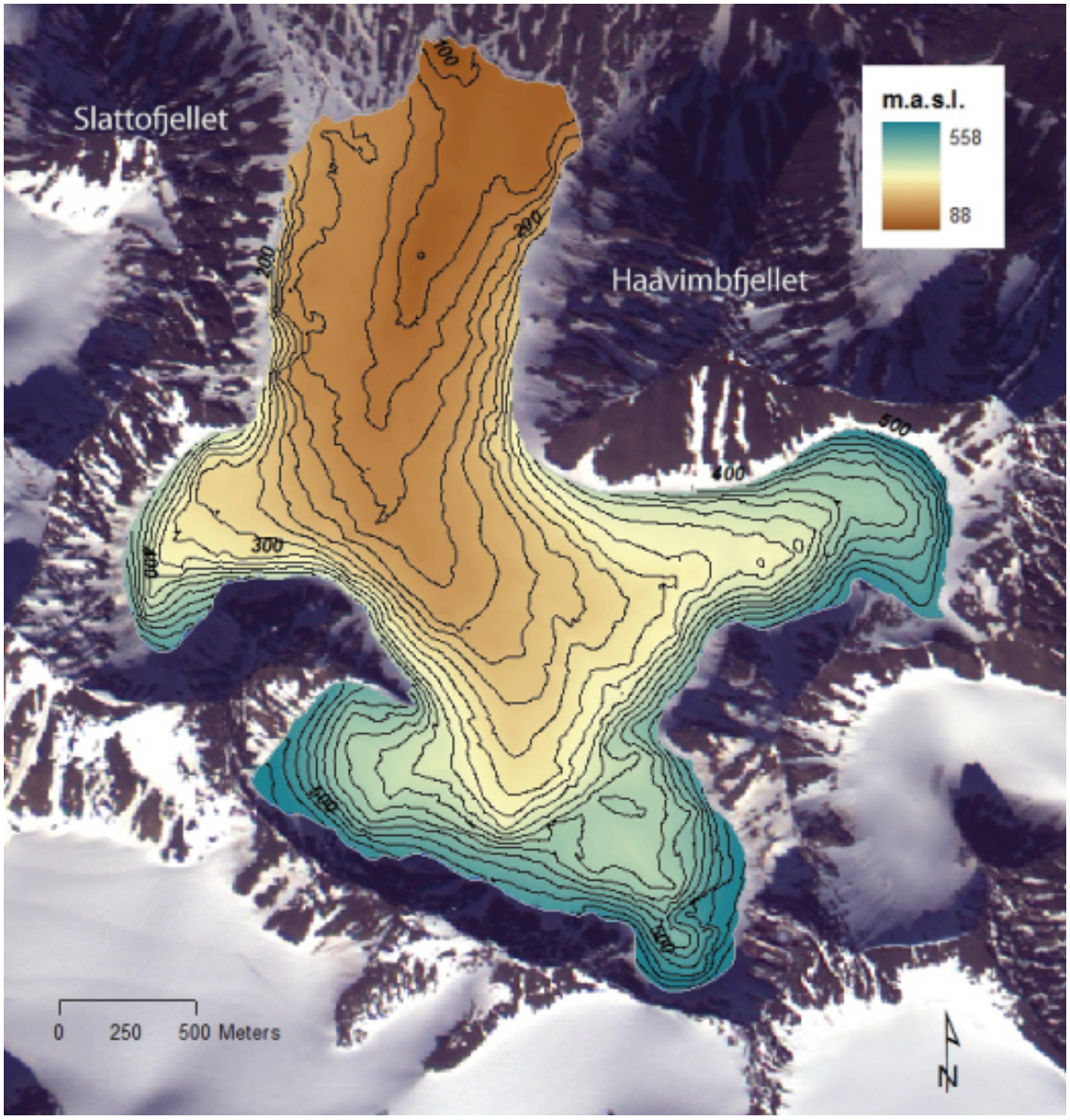

Fig. 11. DEM of the glacier substratum with 20-m spaced contour lines (background image copyright FORMOSAT).

LIST OF TABLES

Cause of error	Volume	Relative error
Ice thickness: ± 1.77 m	0.008 km^3	2.3 %
Glacier area	0.0056 km^3	1.6 %
Snow thickness	9.2×10^{-4} km^3	0.3 %
Electromagnetic wave velocity	0.0042 km^3	1.2 %
Interpolation error	0.040 km^3	11.5 %

TABLE I
SUMMARY OF CONTRIBUTIONS TO GLACIER VOLUME ESTIMATION ERROR. THE SUM OF ALL ERRORS YIELDS TO A 11.9 % ACCURACY.